Dose and Dose-Rate Effects in a Mouse Model of Internal Exposure from 137Cs. Part 2: Integration of Gamma-H2AX and Gene Expression Biomarkers for Retrospective Radiation Biodosimetry

Authors: Shuryak, Igor, Ghandhi, Shanaz A., Turner, Helen C., Weber, Waylon, Melo, Dunstana, et al.

Source: Radiation Research, 196(5) : 491-500

Published By: Radiation Research Society

URL: https://doi.org/10.1667/RADE-20-00042.1

RADIATION RESEARCH **196**, 491–500 (2020)
0033-7587/20 $15.00

DOI: 10.1667/RADE-20-00042.1

Dose and Dose-Rate Effects in a Mouse Model of Internal Exposure from ^{137}Cs. Part 2: Integration of Gamma-H2AX and Gene Expression Biomarkers for Retrospective Radiation Biodosimetry

Igor Shuryak,[a,1] Shanaz A. Ghandhi,[a] Helen C. Turner,[a] Waylon Weber,[b] Dunstana Melo,[c] Sally A. Amundson[a] and David J. Brenner[a]

[a] *Center for Radiological Research, Columbia University Irving Medical Center, New York, New York 10032;* [b] *Lovelace Biomedical, Albuquerque, New Mexico, 87108; and* [c] *Melohill Technology, Rockville, Maryland, 20815*

Shuryak, I., Ghandhi, S. A., Turner, H. C., Weber, W., Melo, D., Amundson, S. A. and Brenner, D. J. Dose and Dose-Rate Effects in a Mouse Model of Internal Exposure from ^{137}Cs. Part 2: Integration of Gamma-H2AX and Gene Expression Biomarkers for Retrospective Radiation Biodosimetry. *Radiat. Res.* 196, 491–500 (2020).

Inhalation and ingestion of ^{137}Cs and other long-lived radionuclides can occur after large-scale accidental or malicious radioactive contamination incidents, resulting in a complex temporal pattern of radiation dose/dose rate, influenced by radionuclide pharmacokinetics and chemical properties. High-throughput radiation biodosimetry techniques for such internal exposure are needed to assess potential risks of short-term toxicity and delayed effects (e.g., carcinogenesis) for exposed individuals. Previously, we used γ-H2AX to reconstruct injected ^{137}Cs activity in experimentally-exposed mice, and converted activity values into radiation doses based on time since injection and ^{137}Cs-elimination kinetics. In the current study, we sought to assess the feasibility and possible advantages of combining γ-H2AX with transcriptomics to improve ^{137}Cs activity reconstructions. We selected five genes (*Atf5*, *Hist2h2aa2*, *Olfr358*, *Psrc1*, *Hist2h2ac*) with strong statistically-significant Spearman's correlations with injected activity and stable expression over time after ^{137}Cs injection. The geometric mean of log-transformed signals of these five genes, combined with γ-H2AX fluorescence, were used as predictors in a nonlinear model for reconstructing injected ^{137}Cs activity. The coefficient of determination (R^2) comparing actual and reconstructed activities was 0.91 and root mean squared error (RMSE) was 0.95 MBq. These metrics remained stable when the model was fitted to a randomly-selected half of the data and tested on the other half, repeated 100 times. Model performance was significantly better when compared to our previous analysis using γ-H2AX alone, and when compared to an analysis where genes are used without γ-H2AX, suggesting that integrating γ-H2AX with gene expression provides an important advantage. Our findings show a proof of principle that integration of radiation-responsive biomarkers from different fields is promising for radiation biodosimetry of internal emitters.

INTRODUCTION

There is an important need for radiation biodosimetry in response to large-scale radiological events such as improvised nuclear device (IND) detonations or nuclear power plant accidents (e.g., Chernobyl or Fukushima) (*1–10*). The primary tasks for biodosimetry involve secondary triage of large numbers of potentially irradiated individuals to identify those with potential radiological injuries, after initial clinical triage, and/or to help estimate radiation doses for other individuals/groups who received less critical/life-threatening doses (*11, 12*). To accomplish this, there is a need to quantitatively reconstruct radiation dose and to inform exposed individuals as quickly as possible about the magnitude of their exposure and potential consequences and treatment options (*13*).

Importantly, situations where radiation biodosimetry can prove useful are not limited to acute external exposures, but include more complex exposure scenarios like inhalation and ingestion of long-lived radionuclides such as ^{137}Cs into the body (*14*). These situations of internal exposure can result in short-term toxicity (radiation sickness) and/or delayed effects such as carcinogenesis (*15–17*). Compared to acute external exposures, internal emitter exposures offer several challenges for biodosimetry-based dose reconstruction, because dose and dose rate from internal exposure change over time in a nonlinear manner due to radionuclide pharmacokinetics (e.g., distribution from blood to various organs, elimination from the body). Dose and dose rate are not independent variables because both depend on the initial administered activity and on time (*18–20*).

Editor's note. The online version of this article (DOI: https://doi.org/10.1667/RADE-20-00042.1) contains supplementary information that is available to all authorized users.

[1] Address for correspondence: Center for Radiological Research, Columbia University, 630 West 168th St., VC-11-234/5, New York, NY, 10032; email: is144@cumc.columbia.edu.

In collaboration with Lovelace Biomedical Research Institute (LBRI; Albuquerque, NM), we developed a mouse model system where various amounts of ^{137}CsCl were injected into the animals, and excretion kinetics, dose rates, doses, γ-H2AX fluorescence (*20, 21*), and transcriptomic (*22, 23*), metabolomic (*24*) and lipidomic (*25*) biomarkers were measured over time after injection. More recently, we used a γ-H2AX end point in peripheral blood mononuclear cells to reconstruct the ^{137}Cs activity after injection with several different ^{137}Cs amounts (*20*). Activity values were converted into radiation doses, using the time since injection and ^{137}Cs pharmacokinetics information. The model-based reconstructions were most accurate between 2–5 days of exposure due to persistent expression of γ-H2AX at these times after ^{137}Cs injection. This work highlighted the feasibility of using γ-H2AX as a biomarker to assess injected ^{137}Cs activity. We proposed that combining γ-H2AX with other biomarkers may have the potential to more accurately reconstruct ^{137}Cs activity and the resulting absorbed dose and biological damage in the blood over a longer period of time.

The additional biomarker we chose was transcriptomics response. Results of the global gene expression profiling analysis are reported in Ghandhi *et al*. (*23*). The goal of this work was to identify genes that could serve as robust and reliable biomarkers of protracted internal radiation exposure. Such genes should have a strong radiation response that is consistent across several radiation studies and is stable over days–weeks after the start of exposure. We also assessed the feasibility and potential advantages of combining such gene expression data with γ-H2AX for reconstructing ^{137}Cs activity.

MATERIALS AND METHODS

Study Overview

Male C57BL/6 mice were injected with varying amounts of ^{137}CsCl, and sacrificed at times from 2 to 14 days later for collection of blood and subsequent measurement of biodosimetry end points, as described elsewhere (*20, 23*). Male mice were used to build on the results of these previous studies, and the data were used as an initial test of gene expression and cytogenetic data integration. All animal studies were conducted at Lovelace Biomedical Research Institute in facilities accredited by the Association for Assessment and Accreditation of Laboratory Animal Care (AAALAC) using protocols approved by the Lovelace Institutional Animal Care and Use Committee (IACUC; approved protocol no. FY15–087).

Gamma-H2AX Fluorescence Measurements

Immunodetection of γ-H2AX was performed according to our previous work reported elsewhere (*20, 21, 26*). Briefly, isolated blood mononuclear cells (MNC) were blocked with 3% bovine serum albumin (BSA; Sigma-Aldrich® LLC, St. Louis, MO) for 30 min at room temperature and incubated with a rabbit polyclonal γ-H2AX (phospho S139) antibody (dilution 1:600; Abcam®, Cambridge, MA), visualized with a goat anti-rabbit Alexa Fluor® 488 antibody (dilution 1:1,000; Invitrogen™, Carlsbad, CA) and counterstained with DAPI in Vectashield® mounting media (Vector® Laboratories, Burlingame, CA). Fluorescent images of cells were captured using an Olympus epifluorescence microscope (Olympus BH2-RFCA; 60× oil immersion objective) and quantification of γ-H2AX yields was determined by measuring the total γ-H2AX nuclear fluorescence per MNC. Data were analyzed using image analysis software described elsewhere (*26*).

Gene Expression Measurements

A brief description is included here of the gene expression results that were the basis for the gene selection for the activity reconstruction algorithm developed in this study. RNA samples from six animals per time point per injection group were used to generate transcriptomic data using Whole Genome Mouse Arrays (Agilent Technologies Inc., Santa Clara, CA), using the recommended manufacturer's protocol. The gene expression data set is deposited in the NCBI Gene Expression Omnibus database (accession no. GSE118616) and is described in detail in Ghandhi *et al*. (*23*).

Selection of Genes for ^{137}Cs Activity Reconstruction

The research strategy was to focus on those genes that have the largest (absolute value) Spearman's correlation coefficients with injected ^{137}Cs activity and near-zero correlation coefficients with time after injection. The search was performed using *R* 3.5.2 software (*27*). We selected the top five genes (*Atf5*, *Hist2h2aa2*, *Olfr358*, *Psrc1* and *Hist2h2ac*), ranked in decreasing order by Spearman's correlation coefficients (all statistically significant at $\alpha = 0.05$ level with Bonferroni correction) with injected activity, for further analysis. Sensitivity calculations using all statistically significant candidate genes (there were eight, shown in the Supplementary_data_genes.scv file in the Supplementary Materials; https://doi.org/10.1667/RADE-20-00042.1.S1) instead of the top five, and comparing the performances of these model variants by Akaike information criterion (AIC), coefficient of determination (R^2) and root mean squared error (RMSE), showed very similar results, so we proceeded with the top five.

We also assessed the dose-response patterns of these five genes in other published studies: 1. Our earlier internal ^{137}Cs study using a single injection activity (*22*) (Dataset: GEO accession no. GSE52690); and 2. Several published studies of acute external irradiation (*28–31*) (Datasets: GEO accession nos. GSE124612, GSE114142, GSE99176). Consistency of dose-response patterns across all/most of these studies would provide improved confidence that the selected genes represent reliable candidates for radiation biodosimetry in a variety of exposure scenarios.

Combining γ-H2AX and Gene Expression Data Sets

Blood samples from eight mice per exposure group were pooled for γ-H2AX analysis, and six mice per group for gene expression analysis, for technical reasons: Due to reduced blood mononuclear cell counts after radiation exposure in a relatively small volume of blood (~100–200 μl) from each mouse, it was necessary for the γ-H2AX assay to pool the blood from several mice to obtain enough cells for robust γ-H2AX analysis. Gene expression data were originally measured for individual mice, with the results being pooled to allow integration with γ-H2AX data.

Consequently, mean injected activity values for the mouse groups differed slightly for the γ-H2AX and gene expression data sets. To combine the data sets for our biomarker integration analysis, the injected activity values were averaged from the γ-H2AX and gene expression studies. The numerical changes from this procedure were very small, since activity values for the exposure groups were modified by only 0.003 to 0.062 MBq, whereas the range of studied non-zero activities was 5.76 to 9.29 MBq.

For the injected activity, γ-H2AX and gene expression measurements, the uncertainties were fairly small on a relative scale, usually a few percentages of the respective means. For injected activity, the range of variations between mouse groups was –3.2% to +4.4% of the mean values. For γ-H2AX fluorescence, standard errors were on

TABLE 1
Five Top-Scoring Genes Selected for the Current Biodosimetry Analysis

Gene symbol	Spearman's correlation with injected activity	*P* value
Atf5	0.88	7.68×10^{-9}
Hist2h2aa2	0.82	5.33×10^{-7}
Olfr358	0.82	5.33×10^{-7}
Psrc1	0.82	6.69×10^{-7}
Hist2h2ac	0.81	8.35×10^{-7}

Notes. These genes had: 1. The largest and most statistically significant Spearman's correlation coefficients with injected activity (*P* value threshold for $\alpha = 0.05$ adjusted by Bonferroni correction was 2.12×10^{-6}); and 2. Near-zero correlation coefficients with time after injection (between –0.24 and +0.10, median = 0.03). As described in Materials and Methods, the gene signal values in each sample, which were used to calculate the correlation coefficients, were $\log_2$-transformed mean intensities for six mice per sample.

average 2.3% of the mean (range: 1.2 to 3.0%). For gene expression, standard errors were on average 11.1% of the mean (range: 3.5 to 23.2%).

Because the signal values ($\log_2$-transformed and normalized) of these top five selected genes were strongly correlated with each other across the samples, each gene was not treated as an independent predictor. The geometric mean of signal values for all five genes (designated as the variable *Net_sig*) was used as a single robust predictor of injection activity. We assessed the reasonableness of this assumption by removing each of the five genes one by one and performing the analysis using the geometric mean of the remaining four genes. Only removal of *Psrc1* significantly reduced R^2 for the resulting model, whereas removal of any of the other genes did not affect R^2 significantly.

Gamma-H2AX mean fluorescence (designated as the variable *gH2AX*, in arbitrary units) was used as the second predictor. Quadratic Net_sig^2 and $gH2AX^2$ terms were also considered to assess potential non-linear relationships. Time after radioactivity injection was the final tested predictor variable. All time points (2–14 days after ^{137}Cs injection) were used in the analysis.

Mathematical Model Development and Fitting

Multimodel inference (MMI) (*32, 33*) using the Akaike information criterion with sample size correction (AICc) was performed using the *glmulti R* package on multiple linear regressions with all possible combinations of these predictor variables (main effects and interactions). Only those predictors that had the highest MMI importance scores were retained for further analysis.

We used the retained predictor variables to construct a three-parameter nonlinear model. The model structure was not intended to represent any specific radiation response mechanisms, which are not yet well known for these genes. It was simply intended to capture the main data patterns and to generate only positive numbers for reconstructed injected activity (unlike linear or polynomial regressions, which can generate negative predictions). The model's performance was assessed by R^2 and RMSE.

Model Testing

The robustness of these metrics was assessed by calculating them not only on the full data set, but also on 100 random 50:50 splits of the data into training and testing halves. Best-fit model parameters obtained on the training data were used to generate model predictions and corresponding R^2 and RMSE values on the testing data.

We quantified the sensitivity of model predictions to ±10% changes in each predictor variable (*gH2AX* or *Net_sig*) by calculating how these changes affect R^2 and RMSE metrics at each time point (2, 3, 5, 7 or 14 days after ^{137}Cs injection), or over all time points combined. Model parameter values were kept constant at best-fit values. Potential time trends for each metric were also assessed using Pearson correlation coefficients with time after injection.

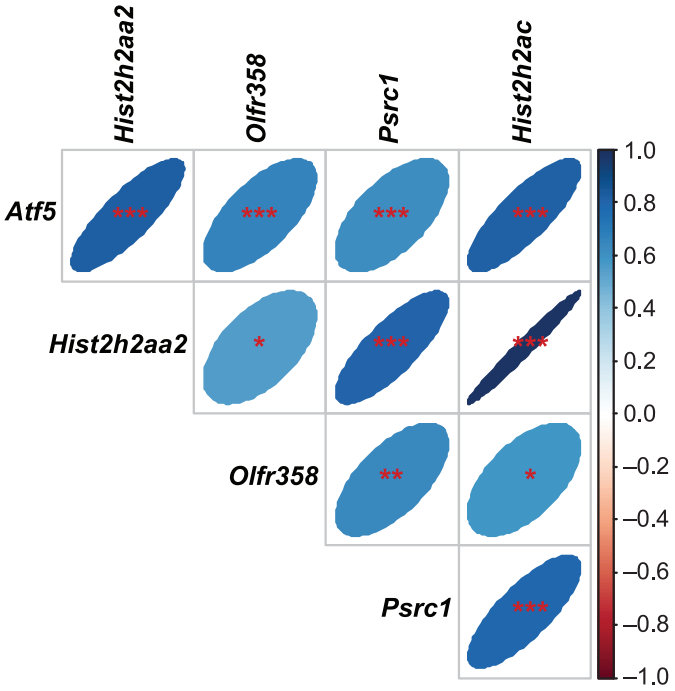

FIG. 1. Matrix of pairwise Spearman's correlation coefficients between the five selected genes with the strongest positive Spearman's correlations with injected activity (Table 1). A color-coded correlation scale is provided on the right side of the plot. Based on the scale, blue ellipses represent positive correlations of a given gene pair, and red ones represent negative correlations. Darker color tones and narrower ellipses represent larger correlation coefficient magnitudes. Red asterisks indicate statistical significance levels for pairwise correlations (intended for visualization only): ***$P < 0.001$, **$P < 0.01$, *$P < 0.05$; where there are no asterisks, $P > 0.05$. There were no negative correlations among gene pairs, so only blue ellipses are shown.

RESULTS

Radiation-Responsive Genes

The top five genes that had large and statistically significant Spearman's correlation coefficients with injected activity and remained stable over time after injection were *Atf5*, *Hist2h2aa2*, *Olfr358*, *Psrc1* and *Hist2h2ac* (Table 1). All the selected genes had similarly-shaped dependences on injected activity that were strongly correlated with each other (Figs. 1–2). Combining them into a single variable by using the geometric mean of the log-transformed gene signals (*Net_sig*) provided a good biomarker for injected activity (Figs. 2–3, Supplementary Fig. S1; https://doi.org/10.1667/RADE-20-00042.1.S2).

As an initial validation, the same polynomial regression model relating *Net_sig* to injected activity (Fig. 3) was applied to an independent data set from our initial ^{137}Cs injection study (*22*). On this data set, the model-based

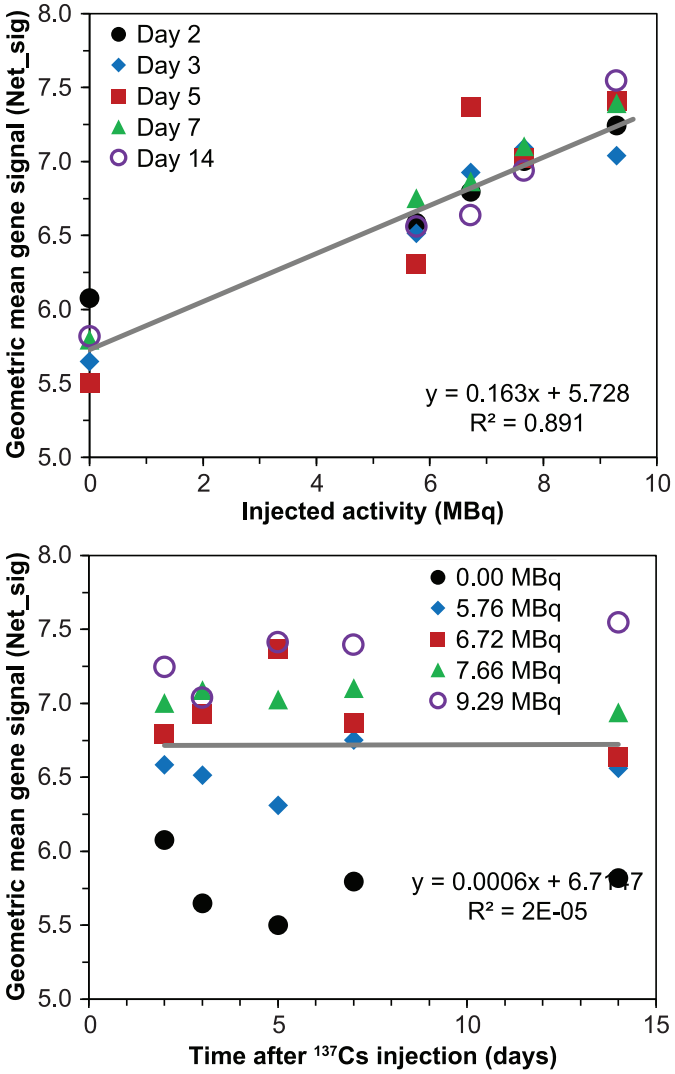

FIG. 2. Dependence of the geometric mean of five selected genes (*Atf5*, *Hist2h2aa2*, *Olfr358*, *Psrc1* and *Hist2h2ac*) on injected ^{137}Cs activity (upper panel) and on time after injection (lower panel). As described in the main text, the genes were selected because they had the largest Spearman's correlation coefficients with injected activity and near-zero correlation coefficients with time. The line represents a linear regression through all data points.

reconstructed activity was 6.51 MBq, whereas the actual value was 7.67 MBq. This error of 1.16 MBq (~15% on a relative scale) is similar to the model's RMSE on the original data set (0.99 MBq). Therefore, the five selected genes performed similarly for activity reconstruction across two independent data sets. The selected genes also tended to increase in expression with increasing radiation dose in studies of acute external irradiation (*28, 31, 34*). These findings further support these genes as reliable candidates for internal emitter biodosimetry.

Integration of Gene Expression with γ-H2AX

Gamma-H2AX fluorescence showed curving dependences for injected activity and time (Fig. 4), which likely reflect

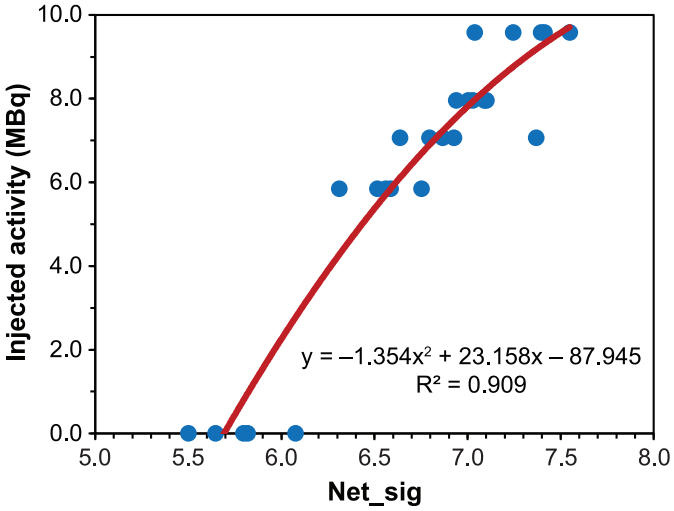

FIG. 3. Polynomial regression for reconstructing injected activity based on *Net_sig*, the geometric mean of five selected genes (*Atf5*, *Hist2h2aa2*, *Olfr358*, *Psrc1* and *Hist2h2ac*). The individual points are mean *Net_sig* at all time points (days 2 to 14) in each injected group.

the kinetics of the biomarker itself as well as changes in the MNC population due to the death of heavily-damaged cells and proliferation of new ones (*20*). To determine the best way to combine γ-H2AX with gene expression, we evaluated all possible combinations of time since injection, *gH2AX*, *Net_sig*, and their quadratic terms and interactions to reconstruct injected activity by multiple linear regression. An importance score based on Akaike information criterion weights was calculated for each predictor variable and interaction term (*32, 33*).

Time and its interaction terms with other variables had the lowest importance scores, <0.012. The analysis of multiple regression combinations was then repeated without time as a variable. This showed that the quadratic *Net_sig*^{2} term and its interactions with other variables now had the lowest

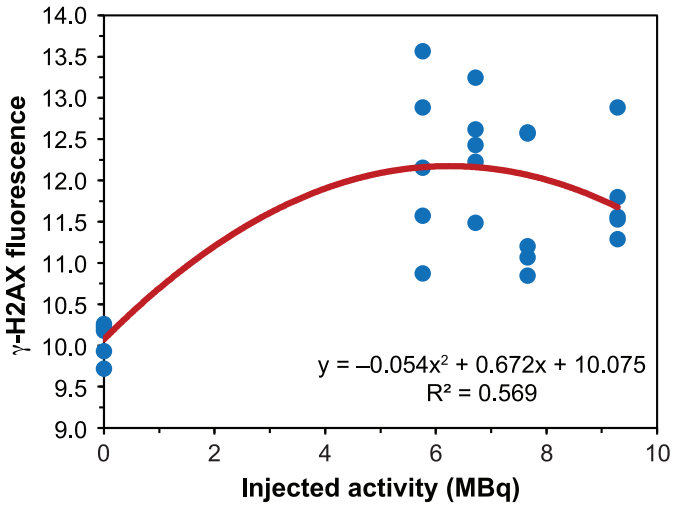

FIG. 4. Relationship between injected activity and γ-H2AX fluorescence (in arbitrary units). The individual points are the mean *gH2AX* signal at all time points in each injected group.

TABLE 2
Robustness Testing Results for the Nonlinear Model that Used γ-H2AX Fluorescence and Geometric Mean of Selected Gene Expression Levels (*Net_sig*) to Reconstruct Injected Activity [Eq. (1)]

Metric	Value for full data set (SE)	Mean value on training data (SD)	Mean value on testing data (SD)
R^2	0.913	0.907 (0.059)	0.883 (0.111)
RMSE (MBq)	0.947	0.879 (0.191)	1.109 (0.266)
Model parameter k_1	16.0 (2.5)	16.6 (3.4)	-
Model parameter k_2	–0.208 (0.034)	–0.216 (0.046)	-
Model parameter k_3	-2.28×10^{-3} (6.17×10^{-5})	-2.26×10^{-3} (7.15×10^{-5})	-

Notes. As described in Materials and Methods, the full data set was randomly split into training and testing halves. The model fits to training data were used to calculate R^2 and RMSE metrics on both training and testing data. This analysis was repeated 100 times. SE = standard error; SD = standard deviation.

importance scores, <0.28. The highest scores of 0.73 and 0.65, respectively, were achieved by two interactions: *Net_sig*×*gH2AX*^{2} and *Net_sig*×*gH2AX*. The main effects of these variables had lower scores, <0.56.

Based on these findings, we developed a nonlinear model using the interactions *Net_sig*×*gH2AX*^{2} and *Net_sig*×*gH2AX* as predictors of injected activity. The model contained three parameters (k_1, k_2 and k_3) and had the following structure, where *gH2AX* represents the γ-H2AX fluorescence signal and *Net_sig* represents the combination of five selected genes:

$$A = \left[\frac{100}{1 + \exp\left[k_1 + k_2 \times Net_{sig} \times gH2AX\right]}\right] \times \exp\left[k_3 \times Net\_sig \times gH2AX^2\right]. \quad (1)$$

As described in Materials and Methods, the model is empirical rather than mechanistically motivated. The goal was to create a parsimonious and easily-applied formalism for activity reconstruction. The model was fitted to the data using robust nonlinear regression (*nlrob* function in *R*), which reduces the influence of outlier data.

Model-Based Reconstructions of Injected ^{137}Cs Activity

Best-fit model parameters and performance metrics (R^2 and RMSE) are presented in Table 2, and model behaviors are plotted in Fig. 5. The model was generally quite accurate in reconstructing the injected activity values (Fig. 6). The R^2 and RMSE metrics remained relatively stable when the model was fitted to one half of the data, which had been randomly selected, and tested on the other half, repeated 100 times (Table 2). Such stability suggests that the model is not strongly over-fitting and is robust to random variations of the data.

Since the γ-H2AX radiation response was stronger at short times (≤5 days) after injection than at longer times (*20*), we calculated RMSE for the current integrated model (Eq. 1) for times ≤5 days on testing data sets. The mean RMSE values were somewhat lower for times ≤5 days than for all times: 1.058 (SD = 0.360) vs. 1.109 (0.266), respectively. However, these differences were small, suggesting that the integrated model had similarly good accuracy across the tested time range (0–14 days after injection). Such similarity of RMSE across time points resulted from the contribution of genes (variable *Net_sig*) because the genes selected for this analysis had stable expression patterns over time.

More detailed examination of model performance metrics R^2 and RMSE over time after ^{137}Cs injection showed that Pearson correlation coefficients with time were 0.34 ($P = 0.58$) and –0.35 ($P = 0.56$) for R^2 and RMSE, respectively. Therefore, both metrics varied somewhat with time, but their variations did not reach statistical significance. These results suggest that the agreement between actual injected activity and model predictions was consistent over all the analyzed time points (up to 14 days after injection).

Sensitivity analysis of model predictions using ±10% changes in each predictor variable (*gH2AX* or *Net_sig*) showed that the sensitivity was similar for each predictor. R^2 values were reduced by 0.22 to 0.33, and RMSE values were increased by 0.99 to 1.37 MBq by 10% perturbations of the predictor variables. These R^2 and RMSE changes were not significantly correlated with time for any of the sensitivity analysis combinations. The Pearson correlation coefficient with time approached statistical significance (–0.83, $P = 0.081$) only for the RMSE metric, when *gH2AX* was increased by 10%. This finding suggests that increasing *gH2AX* causes RMSE to decrease with time, probably because *gH2AX* is a more reliable predictor of injected activity at early times after injection (*20*), but its performance decreases at later times.

The mean absolute errors in activity reconstruction based on the current model [Eq. (1)] over all time points were 2.2-fold smaller than in our previously published analysis using γ-H2AX alone (*20*). This result suggests that integrating γ-H2AX with gene expression provides a significant advantage relative to using γ-H2AX alone ($P = 0.024$ by paired t test comparing absolute error magnitudes). Alternatively, to test whether or not inclusion of *gH2AX* as a predictor improves model performance compared to using genes only, we produced and fitted a model variant which contained only *Net_sig* by eliminating the *gH2AX* variable from Eq. (1) (replacing it with 1). This genes-only model variant had $R^2 = 0.904$ and RMSE = 0.996 MBq, which are worse than these metrics for the original model with both *gH2AX* and *Net_sig* (Table 2). Comparison of these model

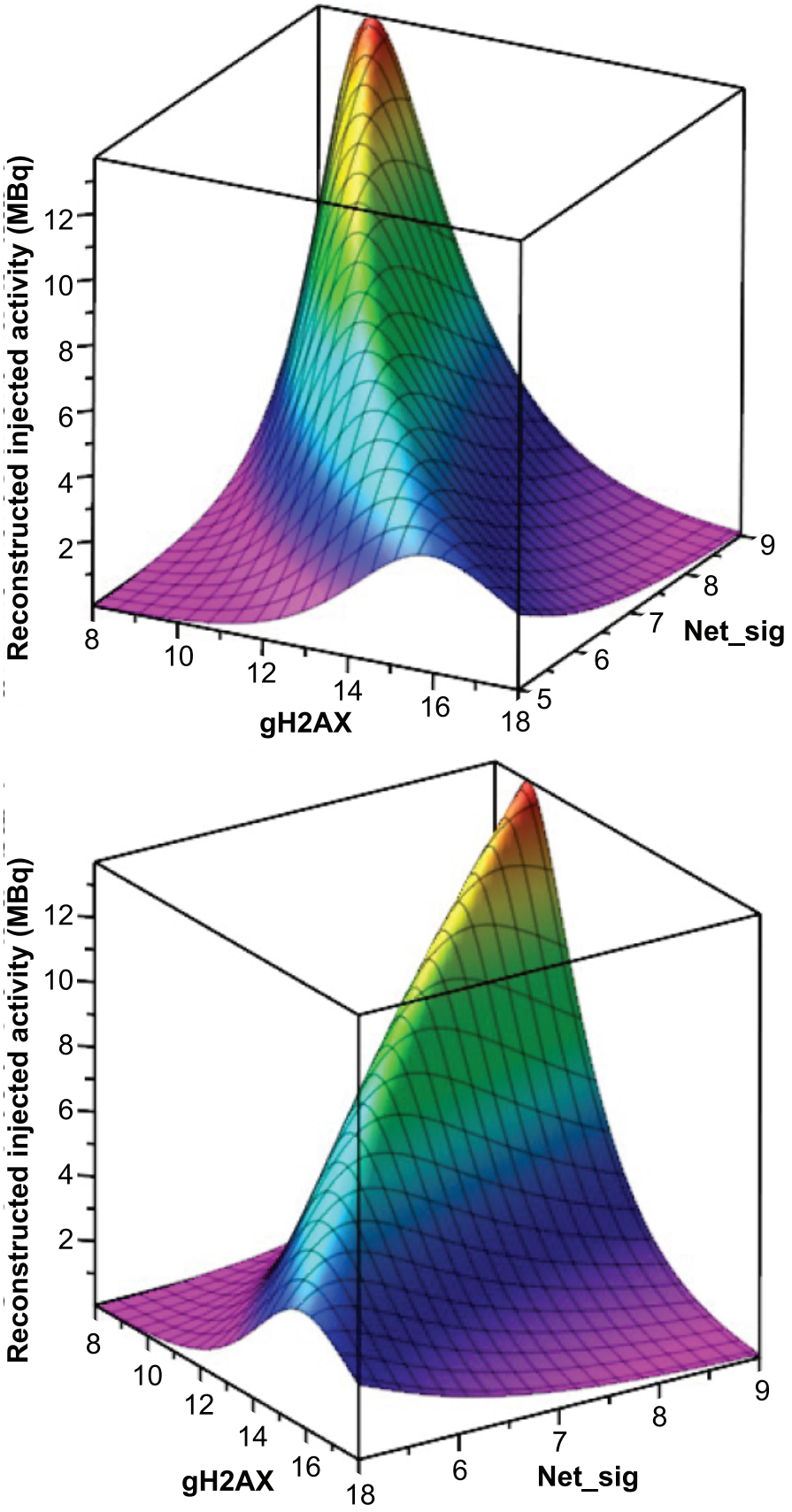

FIG. 5. Behaviors of the nonlinear model that used γ-H2AX fluorescence (*gH2AX*) and geometric mean of selected gene expression levels (*Net_sig*) to reconstruct injected activity (Eq. 1), using best-fit model parameter values (Table 2). The model generates a three-dimensional surface where *gH2AX*, *Net_sig* and reconstructed

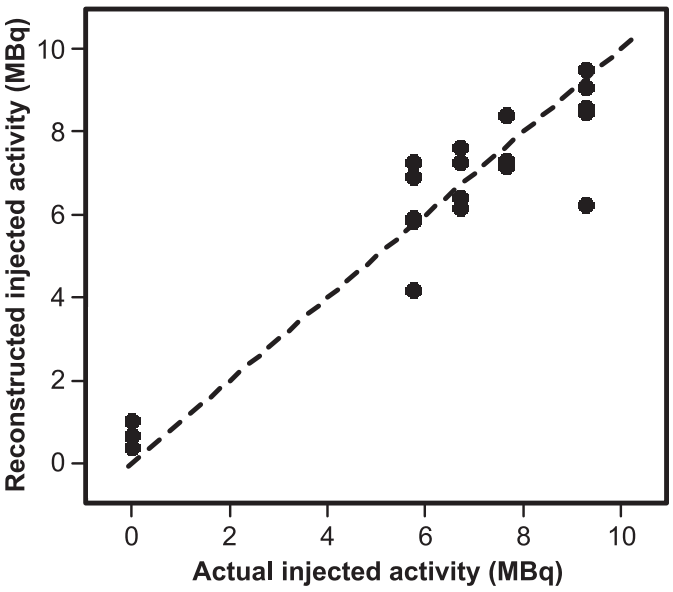

FIG. 6. Comparison of actual and reconstructed mean injected activity values for mouse groups (symbols). The reconstructions were performed using the nonlinear model described in the main text on the entire data set [Eq. (1)]. The dashed line represents the theoretically perfect 1:1 correspondence of actual and reconstructed injected activity values.

variants using Akaike information criterion (AIC) showed that the genes-only model performed worse than the original model by 8.2 AIC units, which translates into an evidence ratio of exp[–8.2/2] $\sim$ 0.016. Therefore, using genes only instead of combining genes with *gH2AX* resulted in significant (evidence ratio $<$0.05) loss of model performance.

DISCUSSION

Radiation biodosimetry is needed for an effective response to large-scale accidental or malicious events involving ionizing radiation (*1–10*). The importance of high-throughput biodosimetry techniques and assays after a large-scale radiological/nuclear event is well recognized (*3, 35–39*). This provides a rationale for using assays such as proteomic, transcriptomic, metabolomic and cytogenetic end points, which can be automated to provide high-throughput biodosimetry approaches (*4, 40–46*). While standard cytogenetic biodosimetry techniques such as the dicentric chromosome (DCA) and micronuclei (CBMN) assays are known for their accuracy, γ-H2AX assay and gene expression assays using qRT-PCR potentially have the advantage of shorter time-to-result and time-to-dose reconstruction because they do not require cell culturing (*47*).

Combining multiple biodosimetric markers is generally thought to improve the performance of dose reconstruction algorithms (*48*). Early work in this area showed that combinations of blood cell counts and serum levels of one or more proteins improved discrimination of individual mice or non-human primates with severe radiation exposure from those without exposure (*49–51*). A similar approach using a small panel of proteins has also been shown to improve dose assessment and prediction of the severity of injury in multiple animal models (*52, 53*). Software platforms, such as MULTIBIODOSE (*54*) and the Biodosimetry Assessment Tool (*55*), have been developed to easily combine the results of various individual assays to produce a single consensus triage dose for use in accidents. Such a multiparametric approach, combining complete blood counts with plasma levels of Flt3, has actually been tested on 63 individuals involved in a radiation accident in Senegal, and was found to give results similar to those from scoring chromosome rings and dicentrics (*56*).

Here we performed a proof-of-principle study showing that integration of radiation-responsive biomarkers using two different assay approaches, gene expression and H2AX protein phosphorylation levels, is promising for radiation biodosimetry of internal emitters. The results suggest that γ-H2AX as well as specific gene signals are strongly correlated with the amount of ^{137}Cs in the body and remain sufficiently stable over several weeks after ^{137}Cs administration. Reconstructed injected activity values can be converted into radiation doses, using the time since injection and known ^{137}Cs pharmacokinetics information, because dose rate is a function of the ^{137}Cs activity remaining in the body at a given time and dose is the time integral of the dose rate (*20*).

The computational strategy selected here to perform the ^{137}Cs activity reconstructions focused on identifying a small number of candidate genes with robust radiation responses and stability over time. The inclusion of multiple genes is thought to strengthen biomarker performance against potential confounding factors or individual variation (*57*).

Most of the genes selected for inclusion in the activity reconstruction biomarker have documented radiation responses in other studies. Two of the genes, *Atf5* (activating transcription factor 5) and *Psrc1* (proline/serine-rich coiled-coil 1) are linked to the *Tp53* signaling network, a central part of the radiation response. *Atf5* is a transcription factor that itself appears to increase radiation survival by abrogating the function of *Tp53*, specifically in blocking radiation-induced p53-dependent apoptosis, as shown in mouse sarcoma cells (*58*). *Psrc1* is a direct transcriptional target of *Tp53*, and is involved in microtubule polymerization (*59*). *Hist2h2aa2* and *Hist2h2ac* encode core nucleo-

←
injected activity are the three axes. For easier visualization, here this surface is shown from two angles of view in the upper and lower panels. This figure graphically presents the interactions between γ-H2AX and gene expression biomarkers in the context of our model.

TABLE 3
Model Performance Metrics at Different Time Points after ^{137}Cs Injection, and for All Time Points Combined

Time after ^{137}Cs injection (days)	R^2	RMSE (MBq)
2	0.87	1.48
3	0.95	0.74
5	0.97	0.59
7	0.97	0.88
14	0.94	0.81
Combined	0.91	0.95

some proteins, involved in wrapping DNA into chromatin, limiting DNA damage and increasing chromatin stability. Many histone genes have been shown to be downregulated in response to DNA damage both via the p53-dependent G_1 checkpoint response (*60*) and through a p53-independent mechanism (*61*). Transcriptomic studies have also shown increased expression of histone 2h2a family genes after radiation exposure in mice (*28*), non-human primates (*62*) and humans (*63*).

The *Olfr358* gene codes for a protein that is predicted to have olfactory receptor activity via G-protein coupled receptor signaling. Genes coding for proteins in this signaling pathway, including numerous members of the *Olfr* family, are often found to be strongly responsive in mouse irradiation studies (*22, 28*). Thus, this likely represents a general signaling response related to stress rather than olfaction. The highly correlated pattern of response for the selected genes suggests they may have a common regulator or signaling pathway, perhaps triggered by sustained DNA damage and *Tp53*-driven transcriptional activation.

To reduce the number of predictors and adjustable parameters, and to alleviate potential problems with multicollinearity of predictors, the five selected genes were not treated as independent predictors, but combined into one predictor variable (*Net_sig*) using the geometric mean of their signal values. The choice of model structure for integrating the gene-based predictor *Net_sig* with γ-H2AX was assisted by information theoretic MMI analysis.

This approach resulted in a simple mathematical model with three adjustable parameters [Eq. (1)]. Because of its simplicity, the model was quite stable to variations in the data such as random splits of the data set into training and testing halves. The limited numbers of model parameters and predictors are reasonable to avoid overfitting, because the data set was small and inter-individual variations were ''smoothed'' due to the technical necessity of pooling the data from multiple samples, so that each analyzed data point represents an average for a group of mice rather than the data from each individual mouse.

While injection of ^{137}Cs into mice provides a useful model for the study of radioactive cesium as an internal emitter, it does present experimental and logistical challenges. Because the mice and all associated biomaterials are radioactively contaminated, they require special handling and costly clean-up and decontamination procedures. The mice must be housed individually to avoid cross-irradiation between animals, and contaminated biospecimens must be analyzed using dedicated equipment (*64, 65*). The recent development of our innovative variable low-dose-rate gamma irradiator (VAriable Dose-rate External irradiatoR; VADER) that can provide external ^{137}Cs irradiations at dose rates below 1 Gy/day (*65*) will allow us to further validate these biomarkers by simulating realistic environmental exposure scenarios. Future work should also be extended to compare the biomarker response of these protracted exposures in female mice.

In summary, this study provided a proof of principle for the feasibility of the following points: 1. Identification of several genes with robust and consistent radiation responses, suitable for biodosimetry of internal emitters; 2. Integration of these gene data with γ-H2AX fluorescence in a simple model framework, with validation of the predictions in an independent study. Based on the results, we conclude that integrating γ-H2AX with gene expression is a promising strategy for radiation biodosimetry of internal emitters and provides a significant advantage relative to using γ-H2AX alone or genes alone, extending assay utility out to at least 14 days after the onset of exposure.

SUPPLEMENTARY INFORMATION

Supplementary materials. Supplementary_data_genes.csv. This file contains the data for all eight candidate genes and their Spearman's correlation coefficients and *P* values with injected activity.

Fig. S1. The relationships between injected activity and gene signal intensity ($\log_2$-transformed mean intensities for six mice per sample) for each of the five selected genes with the strongest positive Spearman's correlations with injected activity (Table 1), and for the geometric mean of these gene levels.

ACKNOWLEDGMENTS

We thank Ms. Aimee Kowell, and the technical staff at the Lovelace Biomedical and Environmental Research Institute for conducting the ^{137}Cs dosing experiment that generated the data used in this study. We also gratefully acknowledge Mr. Shad R. Morton for assistance with the gene expression data and preparation of figures. This work was supported by the National Institute of Allergy and Infectious Diseases (NIAID grant no. U19-AI067773 to the Center for High-Throughput Minimally Invasive Radiation Biodosimetry).

Received: January 31, 2020; accepted: August 13, 2020; published online: October 16, 2020

REFERENCES

1. Garty G, Xu Y, Elliston C, Marino SA, Randers-Pehrson G, Brenner DJ. Mice and the A-bomb: Irradiation systems for realistic exposure scenarios. Radiat Res 2017; 187:465–75.

2. Wang Q, Rodrigues MA, Repin M, Pampou S, Beaton-Green LA, Perrier J, et al. Automated triage radiation biodosimetry: Integrating imaging flow cytometry with high-throughput robotics to perform the cytokinesis-block micronucleus assay. Radiat Res 2019; 191:342–51.
3. Jacobs AR, Guyon T, Headley V, Nair M, Ricketts W, Gray G, et al. Role of a high throughput biodosimetry test in treatment prioritization after a nuclear incident. Int J Radiat Biol 2020; 96:57–66.
4. Rodrigues MA, Beaton-Green LA, Wilkins RC, Fenech MF. The potential for complete automated scoring of the cytokinesis block micronucleus cytome assay using imaging flow cytometry. Mutat Res Toxicol Environ Mutagen 2018; 836:53–64.
5. Vral A, Fenech M, Thierens H. The micronucleus assay as a biological dosimeter of in vivo ionising radiation exposure. Mutagenesis 2011; 26:11–17.
6. Blakely WF, Romanyukha A, Hayes SM, Reyes RA, Stewart HM, Hoefer MH, et al. U.S. Department of Defense Multiple-Parameter Biodosimetry Network. Radiat Prot Dosimetry 2016; 172:58–71.
7. Wojcik A, Oestreicher U, Barrios L, Vral A, Terzoudi G, Ainsbury E, et al. The RENEB operational basis: complement of established biodosimetric assays. Int J Radiat Biol 2017; 93:15–19.
8. Homer MJ, Raulli R, DiCarlo-Cohen AL, Esker J, Hrdina C, Maidment BW, et al. United States Department of Health and Human Services Biodosimetry And Radiological/Nuclear Medical Countermeasure Programs. Radiat Prot Dosimetry 2016; 171:85–98.
9. Coleman CN, Koerner JF. Biodosimetry: Medicine, science, and systems to support the medical decision-maker following a large scale nuclear or radiation incident. Radiat Prot Dosimetry 2016; 172:38–46.
10. Milner EE, Daxon EG, Anastasio MT, Nesler JT, Miller RL, Blakely WF. Concepts of Operations (CONOPS) for biodosimetry tools employed in operational environments. Health Phys 2016; 110:370–9.
11. Garty G, Karam A, Brenner DJ. Infrastructure to support ultra high throughput biodosimetry screening after a radiological event. Int J Radiat Biol 2011; 87:754–65.
12. Grace MB, Moyer BR, Prasher J, Cliffer KD, Ramakrishnan N, Kaminski J, et al. Rapid radiation dose assessment for radiological public health emergencies: roles of NIAID and BARDA. Health Phys 2010; 98:172–8.
13. Akiba S. Epidemiological studies of Fukushima residents exposed to ionising radiation from the Fukushima Daiichi Nuclear Power Plant prefecture–a preliminary review of current plans. J Radiol Prot 2012; 32:1–10.
14. Giussani A, Lopez MA, Romm H, Testa A, Ainsbury EA, Degteva M, et al. Eurados review of retrospective dosimetry techniques for internal exposures to ionising radiation and their applications. Radiat Environ Biophys 2020; 59:357–87.
15. Fushiki S. Radiation hazards in children - Lessons from Chernobyl, Three Mile Island and Fukushima. Brain Dev 2013; 35:220–7.
16. Baverstock K, Williams D. The Chernobyl accident 20 years on: An assessment of the health consequences and the international response. Environ Health Perspect 2006; 114:1312–7.
17. Little MP, Hall P, Charles MW. Are cancer risks associated with exposures to ionising radiation from internal emitters greater than those in the Japanese A-bomb survivors? Radiat Environ Biophys 2007; 46:299–310.
18. Melo DR, Lipsztein JL, Oliveira CAN, Lundgren DL, Muggenburg BA, Guilmette RA. A biokinetic model for 137Cs. Health Phys 1997; 73:320–32.
19. Leggett RW, Eckerman KF. A systemic biokinetic model for polonium. Sci Total Environ 2001; 275:109–25.
20. Turner HC, Lee Y, Weber W, Melo D, Kowell A, Ghandhi SA, et al. Effect of dose and dose rate on temporal gamma-H2AX kinetics in mouse blood and spleen mononuclear cells in vivo following cesium-137 administration. BMC Mol Cell Biol 2019; 20:13.
21. Turner HC, Shuryak I, Weber W, Doyle-Eisele M, Melo D, Guilmette R, et al. Gamma-H2AX kinetic profile in mouse lymphocytes exposed to the internal emitters cesium-137 and strontium-90. PLoS One 2015; 10:e0143815.
22. Paul S, Ghandhi SA, Weber W, Doyle-Eisele M, Melo D, Guilmette R, Amundson SA. Gene expression response of mice after a single dose of 137Cs as an internal emitter. Radiat Res 2014; 182:380–9.
23. Ghandhi SA. Dose and dose rate effects in a mouse model of internal exposure from 137Cs. Part 1: Global transcriptomic responses in blood. Radiat Res 2021: 195;000-000.
24. Goudarzi M, Weber W, Mak TD, Chung J, Doyle-Eisele M, Melo D, et al. Development of urinary biomarkers for internal exposure by cesium-137 using a metabolomics approach in mice. Radiat Res 2014; 181:54–64.
25. Goudarzi M, Weber WM, Mak TD, Chung J, Doyle-Eisele M, Melo DR, et al. Metabolomic and lipidomic analysis of serum from mice exposed to an internal emitter, cesium-137, using a shotgun LC-MS(E) approach. J Proteome Res 2015; 14:374–84.
26. Turner HC, Shuryak I, Taveras M, Bertucci A, Perrier JR, Chen C, et al. Effect of dose rate on residual gamma-H2AX levels and frequency of micronuclei in X-irradiated mouse lymphocytes. Radiat Res 2015; 183:315–24.
27. R Development Core Team 3.0.1. A language and environment for statistical computing. R Found Stat Comput 2013; 1:1.
28. Paul S, Kleiman NJ, Amundson SA. Transcriptomic responses in mouse blood during the first week after in vivo gamma irradiation. Sci Rep 2019; 9:18364.
29. Dressman HK, Muramoto GG, Chao NJ, Meadows S, Marshall D, Ginsburg GS, et al. Gene expression signatures that predict radiation exposure in mice and humans. PLoS Med 2007; 4:e106.
30. Mukherjee S, Laiakis EC, Fornace AJ, Amundson SA. Impact of inflammatory signaling on radiation biodosimetry: mouse model of inflammatory bowel disease. BMC Genomics 2019; 20:329.
31. Rudqvist N, Laiakis EC, Ghandhi SA, Kumar S, Knotts JD, Chowdhury M, et al. Global gene expression response in mouse models of DNA repair deficiency after gamma irradiation. Radiat Res 2018; 189:337–44.
32. Wagenmakers E-J, Farrell S. AIC model selection using Akaike weights. Psychon Bull Rev 2004; 11:192–6.
33. Burnham KP, Anderson DR. P values are only an index to evidence: 20th- vs. 21st-century statistical science. Ecology 2014; 95:627–30.
34. Mukherjee S, Grilj V, Broustas CG, Ghandhi SA, Harken AD, Garty G, et al. Human transcriptomic response to mixed neutron-photon exposures relevant to an improvised nuclear device. Radiat Res 2019; 192:189–99.
35. Terzoudi GI, Pantelias G, Darroudi F, Barszczewska K, Buraczewska I, Depuydt J, et al. Dose assessment intercomparisons within the RENEB network using G0-lymphocyte prematurely condensed chromosomes (PCC assay). Int J Radiat Biol 2017; 93:48–57.
36. Ryan TL, Pantelias AG, Terzoudi GI, Pantelias GE, Balajee AS. Use of human lymphocyte G0 PCCs to detect intra- and inter-chromosomal aberrations for early radiation biodosimetry and retrospective assessment of radiation-induced effects. PLoS One 2019; 14:e0216081.
37. Smith T, Escalona M, Ryan T, Livingston GK, Sanders JT, Balajee AS. Extension of lymphocyte viability for radiation biodosimetry: Potential implications for radiological/nuclear mass casualty incidents. J Cell Biochem 2019; 120:8619–29.
38. Balajee AS, Hande MP. History and evolution of cytogenetic techniques: Current and future applications in basic and clinical research. Mutat Res Toxicol Environ Mutagen 2018; 836:3–12.
39. Garty G, Turner HC, Salerno A, Bertucci A, Zhang J, Chen Y, et

al. The decade of the RABiT (2005–15). Radiat Prot Dosimetry 2016; 172:201–6.

40. Lee Y, Wang Q, Shuryak I, Brenner DJ, Turner HC. Development of a high-throughput gamma-H2AX assay based on imaging flow cytometry. Radiat Oncol 2019; 14:150.

41. Lengert N, Mirsch J, Weimer RN, Schumann E, Haub P, Drossel B, et al. AutoFoci, an automated high-throughput foci detection approach for analyzing low-dose DNA double-strand break repair. Sci Rep 2018; 8:17282.

42. Port M, Ostheim P, Majewski M, Voss T, Haupt J, Lamkowski A, Abend M. Rapid high-throughput diagnostic triage after a mass radiation exposure event using early gene expression changes. Radiat Res 2019; 192:208–18.

43. Brengues M, Paap B, Bittner M, Amundson S, Seligmann B, Korn R, et al. Biodosimetry on small blood volume using gene expression assay. Health Phys 2010; 98:179–85.

44. Taraboletti A, Goudarzi M, Kabir A, Moon B-H, Laiakis EC, Lacombe J, et al. Fabric phase sorptive extraction-A metabolomic preprocessing approach for ionizing radiation exposure assessment. J Proteome Res 2019; 18:3020–31.

45. Chen Z, Coy SL, Pannkuk EL, Laiakis EC, Hall AB, Fornace AJ, et al. Rapid and high-throughput detection and quantitation of radiation biomarkers in human and nonhuman primates by differential mobility spectrometry-mass spectrometry. J Am Soc Mass Spectrom 2016; 27:1626–36.

46. Royba E, Repin M, Pampou S, Karan C, Brenner DJ, Garty G. RABiT-II-DCA: A fully-automated dicentric chromosome assay in multiwell plates. Radiat Res 2019; 192:311–23.

47. Sullivan JM, Prasanna PGS, Grace MB, Wathen LK, Wallace RL, Koerner JF, et al. Assessment of biodosimetry methods for a mass-casualty radiological incident: Medical response and management considerations. Health Phys 2013; 105:540–54.

48. Sproull M, Camphausen K. State-of-the-art advances in radiation biodosimetry for mass casualty events involving radiation exposure. Radiat Res 2016; 186:423–35.

49. Ossetrova NI, Sandgren DJ, Gallego S, Blakely WF. Combined approach of hematological biomarkers and plasma protein SAA for improvement of radiation dose assessment triage in biodosimetry applications. Health Phys 2010; 98:204–8.

50. Blakely WF, Ossetrova NI, Whitnall MH, Sandgren DJ, Krivokrysenko VI, Shakhov A, et al. Multiple parameter radiation injury assessment using a nonhuman primate radiation model-biodosimetry applications. Health Phys 2010; 98:153–9.

51. Bolduc DL, Villa V, Sandgren DJ, Ledney GD, Blakely WF, Bunger R. Application of multivariate modeling for radiation injury assessment: a proof of concept. Comput Math Methods Med 2014; 2014:685286.

52. Blakely WF, Bolduc DL, Debad J, Sigal G, Port M, Abend M, et al. Use of proteomic and hematology biomarkers for prediction of hematopoietic acute radiation syndrome severity in baboon radiation models. Health Phys 2018; 115:29–36.

53. Lee Y, Pujol Canadell M, Shuryak I, Perrier JR, Taveras M, Patel P, et al. Candidate protein markers for radiation biodosimetry in the hematopoietically humanized mouse model. Sci Rep 2018; 8:13557.

54. Jaworska A, Ainsbury EA, Fattibene P, Lindholm C, Oestreicher U, Rothkamm K, et al. Operational guidance for radiation emergency response organisations in Europe for using biodosimetric tools developed in EU MULTIBIODOSE project. Radiat Prot Dosimetry 2015; 164:165–9.

55. Sandgren DJ, Salter CA, Levine IH, Ross JA, Lillis-Hearne PK, Blakely WF. Biodosimetry Assessment Tool (BAT) software-dose prediction algorithms. Health Phys 2010; 99:S171–83.

56. Bertho JM, Roy L. A rapid multiparametric method for victim triage in cases of accidental protracted irradiation or delayed analysis. Br J Radiol 2009; 82:764–70.

57. Bustamante Eduardo M, Popovici V, Imboden S, Aebi S, Ballabio N, Altermatt HJ, et al. Characterization of molecular scores and gene expression signatures in primary breast cancer, local recurrences and brain metastases. BMC Cancer 2019; 19:549.

58. Nishioka T, Miyai Y, Haga H, Kawabata K, Shirato H, Homma A, et al. Novel function of transcription factor ATF5: blockade of p53-dependent apoptosis induced by ionizing irradiation. Cell Struct Funct 2009; 34:17–22.

59. Hsieh S-C, Lo P-K, Wang F-F. Mouse DDA3 gene is a direct transcriptional target of p53 and p73. Oncogene 2002; 21:3050–7.

60. Su C, Gao G, Schneider S, Helt C, Weiss C, O'Reilly MA, et al. DNA damage induces downregulation of histone gene expression through the G1 checkpoint pathway. EMBO J 2004; 23:1133–43.

61. Meador JA, Ghandhi SA, Amundson SA. p53-independent downregulation of histone gene expression in human cell lines by high- and low-let radiation. Radiat Res 2011; 175:689–99.

62. Ghandhi SA, Turner HCHC, Shuryak I, Dugan GOGO, Bourland JD, Olson JDJD, et al. Whole thorax irradiation of non-human primates induces persistent nuclear damage and gene expression changes in peripheral blood cells. PLoS One 2018; 13:e0191402.

63. Paul S, Barker CA, Turner HC, McLane A, Wolden SL, Amundson SA. Prediction of in vivo radiation dose status in radiotherapy patients using ex vivo and in vivo gene expression signatures. Radiat Res 2011; 175:257–65.

64. Wang Q, Pujol-Canadell M, Taveras M, Garty G, Perrier J, Bueno-Beti C, et al. DNA damage response in peripheral mouse blood leukocytes in vivo after variable, low-dose rate exposure. Radiat Environ Biophys 2020; 59:89–98.

65. Garty G, Xu Y, Johnson GW, Smilenov LB, Joseph SK, Pujol-Canadell M, et al. VADER: a VAriable Dose-rate External 137Cs irradiatoR for internal emitter and low dose rate studies. arXiv 1905.04169: